SCIENCE CHINA
Technological Sciences

September 2011 Vol.54 No.9: 2511–2519
doi: 10.1007/s11431-011-4433-x

Time-stepping finite element analysis on the influence of skewed rotors and different skew angles on the losses of squirrel cage asynchronous motors

ZHAO HaiSen[1*], LIU XiaoFang[1], LUO YingLi[1], CHEN WeiHua[2] & Peter BALDASSARI[3]

[1] *School of Electric and Electronic Engineering, North China Electric Power University, Beijing 102206, China;*
[2] *Shanghai SEARI Motor Technology Co. Ltd., Shanghai 200063, China;*
[3] *MagneForce Software System Inc., New York 14075, USA*

Received November 18, 2010; accepted April 13, 2011; published online June 7, 2011

To study the influence of skewed rotors and different skew angles on the losses of squirrel cage asynchronous motors, a 5.5-kW motor was taken as an example and the multi-sliced field-circuit coupled time stepping finite element method (T-S FEM) was used to analyze the axially non-uniform fundamental and harmonic field distribution characteristics at typical locations in the stator and rotor cores. The major conclusions are: firstly the skewed rotor exhibits a decrease in the harmonic copper losses caused by slot harmonic currents in the stator winding and rotor bars. Secondly, the skewed rotor shifts the non-uniform distribution of field in the axial direction, which leads to more severe saturation and an increase in iron losses. The heavier the load, the more pronounced the increase in iron losses. Furthermore, the influences of different skew angles on motor losses are studied systematically, with skew angles from 0.5 to 1.5 stator tooth pitch. It is found that the lowest total loss occurs at 0.8 stator tooth pitch, and the slot harmonics can be decreased effectively.

squirrel cage asynchronous motors, skewed rotors, losses, time-stepping finite element method (T-S FEM)

Citation: Zhao H S, Liu X F, Luo Y L, et al. Time-stepping finite element analysis on the influence of skewed rotors and different skew angles on the losses of squirrel cage asynchronous motors. Sci China Tech Sci, 2011, 54: 2511–2519, doi: 10.1007/s11431-011-4433-x

1 Introduction

In the development of premium motors, numerous design factors can affect motor losses. It is important to analyze the degree of influence of these factors on the motor losses, and to discover effective countermeasures to reduce the motor losses. Generally, skewed rotors are used to weaken the additional torque and noise caused by slot harmonics field in the traditional design of squirrel cage asynchronous motors [1]. In such cases, rotor bar skews over a range of angles in the axial direction, which causes obvious changes in the field distribution compared to motors without skewed rotor bars and further affects the motor losses. Therefore, it is very necessary to carry out a systematic investigation on the influence of skewed rotors on motor losses.

However, it is difficult to directly study the influence of skewed rotors on motor losses using traditional magnetic circuit based analysis. To solve this problem, many researchers have carried out relevant studies on skewed rotors using the Finite Element Method (FEM). Among them, a multi-slice FEM was established in refs. [2, 3], in which the effects of skewed rotors can be taken into account by using 2-D plane field analysis for squirrel cage asynchronous motors. The same multi-slice FEM was applied to interior Permanent Magnet (PM) motors with segmented magnets in ref. [4]. The influence on computed results from different

*Corresponding author (email: zhaohisen@163.com)

discrete methods along the axial direction was studied in ref. [5]. Furthermore, the 3-D finite element method was used to study the performance of the skewed rotor motor in ref. [6]. However, the 2-D multi-slice FEM has been used widely because the 3-D FEM is much more computationally intense.

An investigation on the performance and the iron losses with skewed rotors using 2-D multi-slice FEM for asynchronous motors with different capacities was carried out in refs. [7, 8]. The air-gap field distribution characteristics in the skewed rotor motors was analyzed in refs. [9, 10]. An improved 2-D multi-slice FEM was proposed in refs. [11, 12], taking into account the transverse current between rotor bars, as well as the influence of these currents on the motor losses. However, the validity of the model still needs to be verified. Although numerous studies regarding skewed rotors can be found in literature, there is still a need for further study on the micro-characteristics of the field at typical locations in stator and rotor core as well as its influence on the motor losses. In addition, the influence of different skew angles on motor losses also needs to be studied.

In this paper, a Y132S-4, 5.5 kW motor is taken as an example and the multi-slice field-circuit coupled Time-Stepping Finite Element Method (T-S FEM) is adopted to analyze the fundamental and harmonic field distribution characteristics at a series of locations along stator and rotor core in the axial direction, both qualitatively and quantitatively. Secondly, the influence of skewed rotors on the motor losses under no-load and full-load conditions is analyzed. Finally, a comparison of the influence of different skew angles on motor losses is made. The research results of this paper provide useful references for the design of skewed rotors. Meanwhile the work contributes to the foundation of knowledge for further research on new rotor structures for squirrel cage motors in order to reduce the losses.

2 Multi-slice field-circuit coupled T-S FEM by taking skewed rotor into account

2.1 Multi-slice field-circuit coupled T-S FEM

Due to the non-uniform field distribution inside the motor, the 2-D FEM method cannot be used to study the performance of the asynchronous motor when the rotor is skewed. To solve this problem, a multi-slice method was proposed in refs. [2, 3], where the skewed rotor was divided into certain slices, along the axial direction, and where each of them was treated as a straight rotor motor, as shown in Figure 1.

In Figure 1, the skewed rotor is divided into k slices, and γ is the skew angle. It is shown that the space position angle in each straight rotor slice is $\theta=\gamma/k$. In each of these slices, one only needs to treat the matrix elements that relate to the vector magnetic potential in the finite element model in the same way as a straight rotor [3]. Furthermore, each matrix is

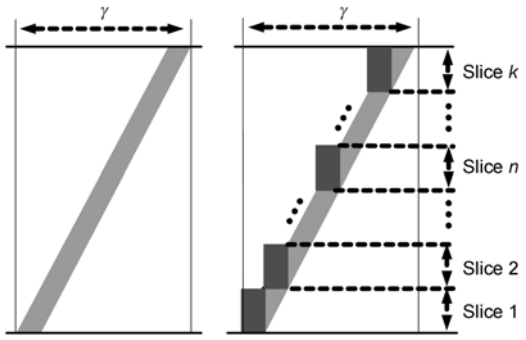

Figure 1 Equivalent model for representation of skew by multi-slice straight rotor.

related to the meshed node coordinate of the redistributed slice along the axial direction, that is, it is dependent on angle θ. Therefore, by taking skewed rotor into account, the multi-slice FEM can be deduced as [13]

$$\begin{bmatrix} \boldsymbol{K}_{\mathrm{A}(1,\theta)} & 0 & 0 & 0 & \boldsymbol{K}_{\mathrm{s}(1,\theta)} & \boldsymbol{K}_{\mathrm{r}(1,\theta)} \\ 0 & \boldsymbol{K}_{\mathrm{A}(2,\theta)} & 0 & 0 & \boldsymbol{K}_{\mathrm{s}(2,\theta)} & \boldsymbol{K}_{\mathrm{r}(2,\theta)} \\ 0 & 0 & \cdots & 0 & \cdots & \cdots \\ 0 & 0 & 0 & \boldsymbol{K}_{\mathrm{A}(k,\theta)} & \boldsymbol{K}_{\mathrm{s}(k,\theta)} & \boldsymbol{K}_{\mathrm{r}(k,\theta)} \\ 0 & 0 & 0 & 0 & \boldsymbol{R}_{\mathrm{s}} & 0 \\ 0 & 0 & 0 & 0 & 0 & \boldsymbol{R}_{\mathrm{r}} \end{bmatrix} \begin{bmatrix} \boldsymbol{A}_{(1)} \\ \boldsymbol{A}_{(2)} \\ \cdots \\ \boldsymbol{A}_{(k)} \\ \boldsymbol{I}_{\mathrm{s}} \\ \boldsymbol{I}_{\mathrm{r}} \end{bmatrix}$$

$$+ \begin{bmatrix} \boldsymbol{D}_{\mathrm{A}(1,\theta)} & 0 & 0 & 0 & 0 & 0 \\ 0 & \boldsymbol{D}_{\mathrm{A}(2,\theta)} & 0 & 0 & 0 & 0 \\ 0 & 0 & \cdots & 0 & 0 & 0 \\ 0 & 0 & 0 & \boldsymbol{D}_{\mathrm{A}(k,\theta)} & 0 & 0 \\ \boldsymbol{D}_{\mathrm{s}(1,\theta)} & \boldsymbol{D}_{\mathrm{s}(2,\theta)} & \cdots & \boldsymbol{D}_{\mathrm{s}(k,\theta)} & \boldsymbol{R}_{\mathrm{s}} & 0 \\ \boldsymbol{D}_{\mathrm{r}(1,\theta)} & \boldsymbol{D}_{\mathrm{r}(2,\theta)} & \cdots & \boldsymbol{D}_{\mathrm{r}(k,\theta)} & 0 & \boldsymbol{R}_{\mathrm{r}} \end{bmatrix} \begin{bmatrix} \boldsymbol{A}_{(1)} \\ \boldsymbol{A}_{(2)} \\ \cdots \\ \boldsymbol{A}_{(k)} \\ \boldsymbol{I}_{\mathrm{s}} \\ \boldsymbol{I}_{\mathrm{r}} \end{bmatrix}' = \begin{bmatrix} 0 \\ 0 \\ 0 \\ 0 \\ \boldsymbol{U}_{\mathrm{S}} \\ 0 \end{bmatrix}. \quad (1)$$

In eq. (1), $\boldsymbol{K}_{\mathrm{A}(n,\theta)}$ is the so-called stiffness matrix of field equations. $\boldsymbol{K}_{\mathrm{s}(n,\theta)}$ and $\boldsymbol{K}_{\mathrm{r}(n,\theta)}$ are the coupled matrix between the nodal vector magnetic potential and the relevant current terms in the equation of the stator and rotor circuit. $\boldsymbol{D}_{\mathrm{A}(n,\theta)}$, $\boldsymbol{D}_{\mathrm{s}(n,\theta)}$ and $\boldsymbol{D}_{\mathrm{s}(n,\theta)}$ are the matrices that correspond to the derivative terms of nodal vector magnetic potential in the field equation and stator and rotor circuit equations, respectively. $\boldsymbol{A}_{(n)}$ is the nodal magnetic potential vector. Among the above variables, n stands for the corresponding matrix (n=1,2,…, k) of the nth straight rotor, and each matrix is a function of skew angle θ. $\boldsymbol{I}_{\mathrm{s}}$ and $\boldsymbol{I}_{\mathrm{r}}$ are the vector of stator currents and rotor end ring currents, respectively. " ′ " is the symbol of derivation, standing for the derivation of each state variable with respect to time. $\boldsymbol{U}_{\mathrm{s}}$ is the matrix of supply voltages.

After rearranging eq. (1), the multi-slice field-circuit coupled T-S FEM equation under rotor skewing condition can be illustrated as [13]

$$\boldsymbol{KX} + \boldsymbol{DX}' = F. \quad (2)$$

In eq. (2), $\boldsymbol{K}$ and $\boldsymbol{D}$ are coefficient matrices taking into ac-

count the contributions of each slice. $\boldsymbol{X}$ is the state variable, including nodal vector magnetic potential, stator current and rotor end ring current. $\boldsymbol{F}$ is the exciting term composed of supply voltages. The backwards difference Euler method is used to discretize eq. (2), and the initial value of each state variable is set to zero. Then, the value of each state variable at each moment can be obtained by solving the nonlinear algebraic equations. The essential information of the 5.5 kW motor is as below: the stator and rotor slot numbers are 36 and 32, respectively; the rotor bars skew over a stator tooth pitch (l_{tp}); the skewed rotor is evenly divided into 5 slices along the axial direction.

2.2 FEM based loss computation method and experiment validation

In computing motor losses by T-S FEM, the losses mainly include stator copper losses, rotor copper losses and iron losses. The stator and rotor copper losses can be computed with the method in refs. [14, 15], by which the fundamental and harmonic copper losses can be computed conveniently. Iron losses can be computed by the model presented by Bertotti in 1988 [16]. The effectiveness of this model has been verified and applied widely [13−17].

For the 5.5 kW motor used in this paper, the computed and tested stator copper losses are 60 W and 62 W respectively, and the computed and tested iron losses are 117 W and 134 W respectively. The test method for no-load iron loss computation is in accordance with method B recommended by GB/T 1032-2005 [18]. Moreover, the tested iron losses also include additional copper loss in the rotor bars but the computed losses are the real losses in stator and rotor core. With the method in refs. [14, 15], no-load rotor copper losses of the 5.5 kW motor can be computed to be 4W. The sum of the computed iron and copper losses in the rotor bars is 121 W, which is nearly the same as the tested no-load iron losses. Furthermore, it is noticed that the losses caused by the transverse current between rotor bars, losses in cramp and the additional fundamentsal frequency loss in the motor base and end covers are not considered, therefore the value of the computed losses is slightly low. However, those losses are reflected indirectly to a certain extent through the main field variables obtained by 2-D FEM. Therefore, the method adopted in this paper is quite convincing and feasible.

3 Distribution characteristics of field inside the motor with skewed rotor along axial direction

3.1 Qualitative analysis in theory

With a straight rotor, the field caused by the stator and rotor currents distributes uniformly along the axial direction. Demagnetizing effects of the rotor field with respect to the stator field is uniform in all respects, causing the overall field distribution to be uniform along the axial direction. At the same time, the core saturation and the amplitude of the fundamental and harmonic flux densities are also equal along the axial direction. Therefore, the detailed analysis of the axial field distribution characteristics in a motor with a straight rotor is not necessary.

Qualitative analysis on the axial distribution characteristics of the field inside the motor with a skewed rotor from classical theory is as follows. In the analysis, it is assumed that the motor is operated with a constant load under rated voltage condition. In this stage of analysis, only the qualitative estimation on the fundamental field is taken into account. This is due to the fact that there is a greater difference of field phase shift along the axial direction between the harmonics and fundamentals. The influence of skewed rotors on harmonics fields is then analyzed subsequently by using the T-S FEM quantitative analysis (see details in Section 3.2). The estimated field caused by the stator and rotor currents and their variations along axial direction is given in Figure 2, which can be further stated as follow.

1) The fundamental field caused by stator currents distributes uniformly along the axial direction, as shown in Figure 2(a). The flux density amplitude and phase angles at locations a, b and c are all the same, namely, $B_a=B_b=B_c$ and $\alpha_a=\alpha_b=\alpha_c$.

2) The fundamental field caused by rotor currents skews over a stator tooth pitch along axial direction. Although the amplitude of the fundamental flux density at different locations is still the same along the axial direction (because the current in rotor bars is the same), there are few differences among their phase angles along axial direction, as shown in Figure 2(b). It can be seen that the flux density amplitudes of locations d, e and f are still the same, but their phase angles are not, that is, $B_d=B_e=B_f$, $\alpha_d>\alpha_e>\alpha_f$.

3) Since the field caused by the rotor current skews over a stator tooth pitch, the demagnetizing effect of the field caused by rotor current with respect to the field caused by the stator current gradually reduces along the axial direction. As a consequence, the resultant field distributes non-uniformly along the axial direction. The distribution characteristics of the resultant fundamental field are shown in Figure 2(c). It can be seen that the flux density amplitudes of locations g, h and i are reduced in proper sequence and the phase angles in different locations are also different, that is, $B_g>B_h>B_i$ and $\alpha_g>\alpha_h>\alpha_i$.

In conclusion, when considering a skewed rotor motor, the demagnetizing effect of the field caused by the rotor current will lead to that the flux density amplitude of resultant field distributes non-uniformly. Specifically, it gradually increases along the axial direction as shown in Figure 2(c). The influence of this phenomenon on core saturation depends on whether the rotor current is large or small, which itself depends upon the load condition. Therefore, the conclusion is as follows. With light load, the rotor current is smaller and the demagnetizing effect of the field caused by rotor current

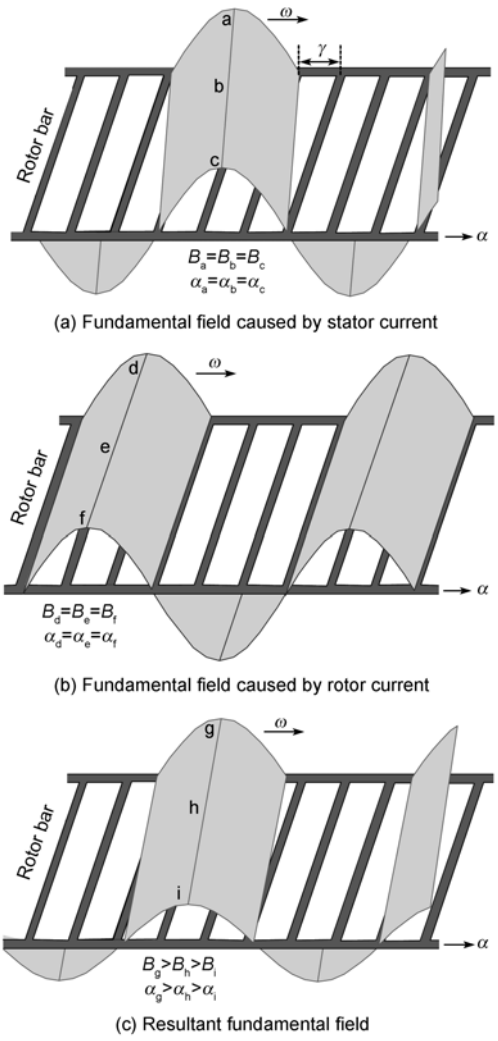

Figure 2 Distribution characteristics of fundamental field with skewed rotors.

on the field caused by the stator current is smaller, and the change of core saturation along axial direction is smaller. With heavy load, rotor current is significantly increased, the demagnetizing effect of the field caused by stator current is more severe, and the increase in core saturation along the axial direction is more pronounced.

3.2 Quantitative analysis based on the multi-slice T-S FEM

3.2.1 Selection of typical locations of stator and rotor core

The 3-D structure of the 5.5kW motor used in this paper is given in Figure 3. To systematically analyze the field distribution characteristic inside the stator and rotor core, Figure 3 chooses 5 typical locations at different axial positions. Among them, S1–S5 are 5 locations inside the stator tooth top area along the axial direction. S6–S10 are 5 locations inside stator tooth body area along the axial direction. S11–S15 are 5 locations inside the yoke area. It is considered that the rotor iron losses are mainly caused by field slot harmonics and are concentrated in rotor tooth top area [13], so 5 locations in certain tooth top areas are chosen to analyze this slot harmonic field, they are listed at R1–R5 in Figure 3. Furthermore, note that we are focused on the distribution characteristics of the field along the *Z* direction. To reveal distribution characteristics of the field inside the motor, only the fundamental and harmonic flux density amplitudes at different locations along the axial direction are studied. Most notably the time variation of flux density details is not analyzed.

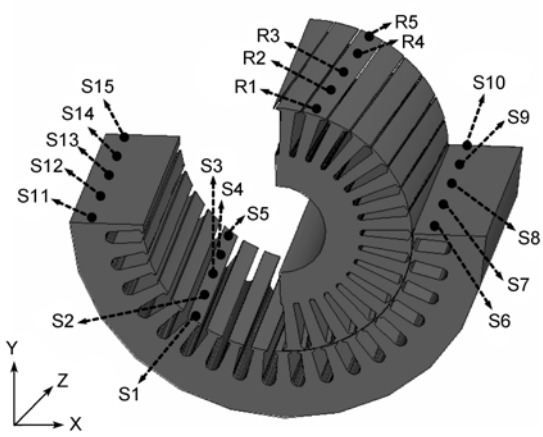

Figure 3 Typical locations of stator and rotor core.

3.2.2 Distribution characteristics of the fundamental field along the axial direction

As stated above, the influence of a skewed rotor on a motor's fundamental field closely relates to the load condition. Further analysis on the variation of the fundamental field inside the motor in the axial direction is carried out by using the T-S FEM in this section. The changing characteristics of fundamental flux density amplitude at different locations on the stator core along the *Z* direction under no-load and full-load conditions are given in Figures 4–6. Among them, B_m is the amplitude of the flux density, B_r and B_t are the respective radial and stangential flux density components. The conclusions are as follows.

1) The demagnetizing effect of the rotor field is smaller under no-load condition. No obvious changes of fundamental flux density amplitude (radial and tangential) occur along the axial direction at locations S1–S5, S6–S10 and S11–S15, as shown in Figures 4(a), 5(a) and 6(a).

2) The demagnetizing effect of the rotor field is more obvious under full-load condition. Fundamental flux density amplitudes (radial and tangential) along axial direction increase in proper sequence at locations S1–S5, S6–S10 and S11–S15, as shown in Figures 4(b), 5(b) and 6(b).

3.2.3 Distribution characteristics of main harmonic field along axial direction

The demagnetizing effect of the rotor field is smaller under

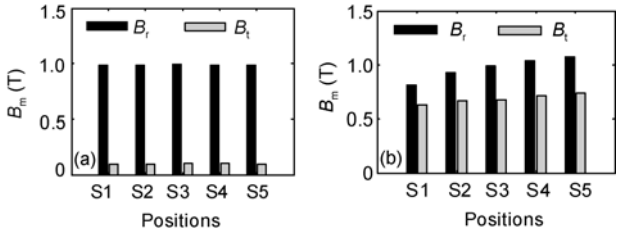

Figure 4 Fundamental flux density amplitude in locations S1–S5 under no-load and full-load conditions. (a) No-load; (b) full-load.

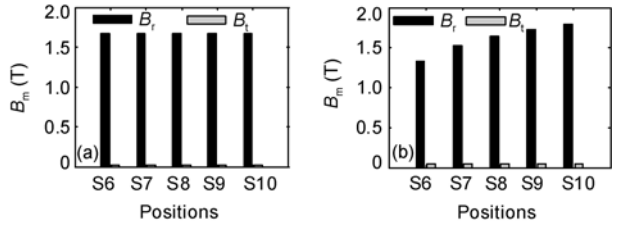

Figure 5 Fundamental flux density amplitude in locations S6–S10 under no-load and full-load conditions. (a) No-load; (b) full-load.

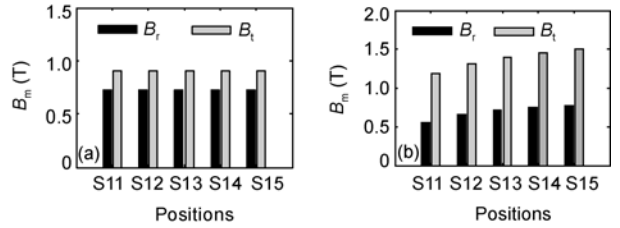

Figure 6 Fundamental flux density amplitude in locations S11–S15 under no-load and full-load conditions. (a) No-load; (b) full-load.

no-load condition, so the distribution characteristics of the harmonic field along the axial direction are expected to be similar to the characteristics of the fundamental field. Therefore, only the distribution characteristics of the harmonic field under full-load condition are analyzed. Based on the theoretical analysis, it is found that, due to core saturation, the harmonic field inside the stator core is mainly a 3rd harmonic field; and the harmonic field in the stator and rotor tooth top area is mainly including slot harmonic due to slotting. Therefore, only the harmonic field with those main orders is studied. To embody the influence of phase shift on the harmonic field along the axial direction, the treatment method for harmonic field analysis is different from that for the fundamental field (radial and tangential directions), in which the vector summation of harmonic fields of different orders is carried out first and then the amplitude of each harmonic component is obtained. The computation results are given in Figure 7, and it can be concluded that:

1) The amplitude of the 3rd harmonic flux density at the stator tooth top (S1–S5) and yoke (S11–S15) along the *Z* direction increases in proper sequence, as shown in Figures 7(a) and 7(c). However, the 3rd harmonic field on the tooth body locations (S6–S10) reduces initially and then increases, as shown in Figure 7(b). After further analysis on the 5th and 7th harmonic fields, it is found that no obvious regular law of flux density amplitude in different stator locations can be drawn.

2) A slight fluctuation of flux density amplitude happens at the stator tooth top locations S1–S5 along the *Z* direction, and the flux density amplitude at the rotor tooth top locations R1–R5 is increased in the proper sequence. Through further analysis on the distribution characteristics of slot harmonics at additional locations, it is found that flux density amplitude of the slot harmonics increases along the axial direction in certain areas. However, it may reduce and even fluctuates in other areas. Therefore, there is no regular law for distribution characteristics of the harmonic field.

The reason for the above phenomena can be explained as follows: the influence of rotor skew on the distribution characteristics of harmonic fields along the axial direction mainly depends on the phase shift of the harmonic field along the axial direction. As the wavelength of harmonic field becomes shorter, there are obvious phase angle differences along the axial direction, which leads to the non-uniform distribution of harmonic fields along the axial direction. The above analysis is also suitable for the no-load condition. Apparently, there is no existing theory to address the variation of the fields along the axial direction of the motor as well as the influence on the iron losses of the motor. In this work, the results of iron losses computed using the multi-slice T-S FEM showed that the non-uniform distribution of the harmonic field does not cause obvious variations of iron losses at the given locations along the axial direction as the fundamental field does. However, the iron losses on each slice are still increased to certain extent, that is, there are no obvious differences of the losses caused by the harmonic field along the axial direction with a skewed rotor, and the total iron losses are still larger than those of a motor with a straight rotor. Detailed instruction about the loss values is given in Section 4.

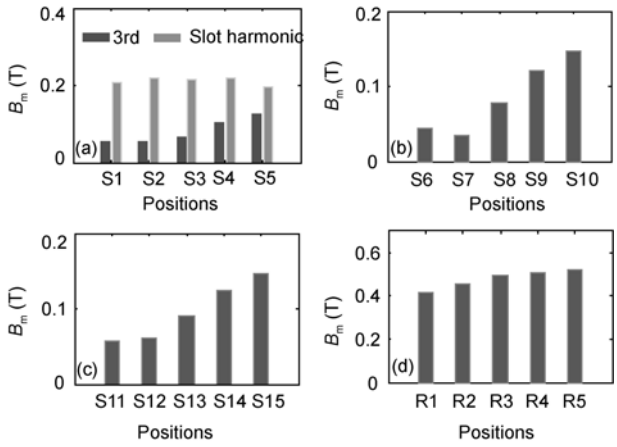

Figure 7 Harmonic flux density amplitude in typical stator and rotor core locations with skewed rotor. (a) The 3rd harmonic and slot harmonic at S1–S5; (b) the 3rd harmonic at S6–S10; (c) the 3rd harmonic at S11–S15; (d) slot harmonic at R1–R5.

4 Influence of skewed rotor on motor losses

4.1 Influence of skewed rotor on the losses under no-load condition

The losses of a 5.5-kW motor with a straight rotor and a skewed rotor under no-load condition are computed with a multi-slice T-S FEM, their comparison is shown in Table 1. The symbol "–" means that the loss value is below 1 W, which can be ignored for the size of the motor. The conclusions are as follows.

1) A skewed rotor can reduce harmonic copper loss in the stator winding and rotor bars. Comparison between the results from the straight and skewed rotors shows that the stator fundamental copper loss is not much different in the two cases, which are 56 W and 57.9 W. However, there is an obvious difference between the stator and rotor harmonic copper loss. With skewed rotors, the stator harmonic copper loss is reduced from 12.5 W to 4 W, and the rotor harmonic copper loss is reduced from 33.9 W to 4 W.

2) With a skewed rotor, the iron losses distribute uniformly along the axial direction. Stator iron loss on each slice is about 18.5 W, and the rotor iron loss on each slice is about 5 W. This corresponds to the results in Section 3.

3) Compared to a straight rotor, the iron losses of the skewed rotor are slightly increased. This can be explained as follows: the fundamental flux density amplitude under no-load condition is basically constant along the axial direction. The stator fundamental iron losses for a straight rotor and a skewed rotor are close to each other, which is approximately 74 W (due to limited space in the table, the stator fundamental iron loss was not listed). Therefore, the non-uniform distribution of the harmonic field leads to the increase in iron losses.

4.2 Influence of skewed rotor on the losses under full-load condition

The comparison of motor losses for a straight rotor and a skewed rotor under full-load condition is given in Table 2. The conclusions are:

1) Similar to the no-load condition, a skewed rotor can reduce harmonic copper loss.

2) Stator iron loss with skewed rotors increases along the axial direction, as shown in Table 2. The stator iron loss on each slice increases from 21.3 W to 28 W. The main reason for this phenomenon has been analyzed in Section 3, namely, the fundamental flux density amplitude increases in each sliced section along the axial direction. Meanwhile, iron losses caused by the rotor harmonic field with skewed rotor are higher than those with a straight rotor, though there is not much difference in the loss values from different slice sections along the axial direction.

3) Under full-load condition, the iron losses are obviously higher than that under no-load condition. According to classical theory, at full-load, the stator current rises significantly and the voltage drops due to winding resistance and leakage reactance increases. This causes the induced electromotive force (EMF) of the stator winding to decrease slightly. Therefore, the iron losses caused by the fundamental field reduce slightly in comparison with those under no-load condition [19]. The computed iron losses show that, under full-load condition, the fundamental iron loss is 69 W, which is slightly lower than the fundamental iron loss of 74 W under no-load condition. However, the harmonic iron loss related to the harmonic field caused by the stator and rotor currents increases significantly. This makes the total iron losses under full-load condition higher than the iron losses under no-load condition.

In conclusion, the skewed rotor reduces the harmonic copper loss caused by the stator and rotor harmonic currents, but at the same time causes the non-uniform distribution of flux density along the axial direction. This results in more severe saturation in the stator and rotor cores. As expected, the increase in iron loss depends mainly on load condition.

Table 1 No-load losses comparison of 5.5 kW motor with straight and skewed rotor

	Total losses (W)	Stator copper loss (W)		Rotor copper loss (W)		Stator iron loss (W)					Rotor iron loss (W)				
		F	H	F	H	S1	S2	S3	S4	S5	S1	S2	S3	S4	S5
Skew	181	56	4	–	4	18.5	18.7	18.5	18.6	18.5	4.7	4.8	5.1	4.9	4.7
Straight	209.8	57.9	12.5	–	33.9			89.5					16		

F, Fundamental loss; H, harmonic loss; S, slice.

Table 2 Full-load losses comparison of 5.5kW motor with straight and skewed rotor

	Total losses (W)	Stator copper loss (W)		Rotor copper loss (W)		Stator iron loss (W)					Rotor iron loss (W)				
		F	H	F	H	S1	S2	S3	S4	S5	S1	S2	S3	S4	S5
Skew	589.8	286	2.3	114	15.2	21.3	22.9	25.4	27.3	28	9.9	9.1	9.1	9.4	9.9
Straight	635.8	283	24.7	117	81.4			99.4					30.6		

F, Fundamental loss; H, harmonic loss; S, slice.

5 Influence of different skew angles on motor losses

5.1 Influence of different skew angles on the losses under no-load condition

In the above analysis, one can see that the skewed rotor reduces the stator and rotor harmonic copper loss caused by slot harmonics, but causes an increase of iron losses due to the increased core saturation. Therefore, for a given motor, there may be an ideal skew angle to reduce the slot harmonics efficiently while minimizing the total losses. However, as slot combination is not always the same for motors of different types, it is not practical to obtain a general method to choose an optimized angle. For the 5.5 kW motor in this paper, the influence of different skew angles on the motor losses was obtained easily by using the T-S FEM. The curves of the influence of different skew angles on each loss term under no-load condition were computed and the results are shown in Figure 8. In the figure, the abscissa stands for different skew angles (γ), which can be represented by different stator tooth pitches (that is l_{tp}), and γ= $0.5l_{tp}$–$1.5l_{tp}$. Through analyzing the loss-variation curve, we can see the following:

1) There is no obvious influence on the stator fundamental copper loss and iron losses for different skew angles. The reason is that the demagnetizing effect of the rotor field is smaller under no-load condition and there is no obvious change of fundamental field along the axial direction.

2) The stator and rotor harmonic copper loss decreases as skew angle increases. This is due to the fact that the slot harmonic EMF in the rotor bars reduces with an increasingly skewed rotor.

3) Stator harmonic iron loss increases initially, and then decreases when the skew angle is greater than $1.1l_{tp}$. Initially, the non-uniform distribution of harmonic field under the no-load condition leads to an increase in iron losses; however, as the skew angle increases further the stator and rotor harmonic current reduces and the iron losses caused by the harmonic currents reduce accordingly. The interactions of these two factors lead to the above phenomenon.

4) As for the rotor harmonic iron loss, the overall variation is that it increases as the skew angle increases. However, the increase tends to be gentle when the skew angle becomes greater than $0.8l_{tp}$. The reason is that, the increase of rotor harmonic iron loss depends on non-uniform distribution of harmonic fields along the axial direction, which is affected by two factors. The first is rotor current, and the second is the skew angle. The higher rotor current causes a stronger demagnetizing effect. Similarly, under the same rotor current, the degree of non-uniform distribution of the harmonic field increases as the skew angle increases. However, under no-load condition, a demagnetizing effect of the rotor field becomes relatively weak and the degree of non-uniform distribution of the harmonic field mainly depends on the skew angle. Meanwhile the rotor harmonic current reduces as the skew angle increases. This will further reduce the demagnetizing effect of the rotor field and lead to the reduction of iron losses. The interaction of the above two factors causes the total losses to increase substantially when the skew angle is $0.5l_{tp}$–$0.7l_{tp}$ and less so when skew angle becomes greater than $0.7l_{tp}$.

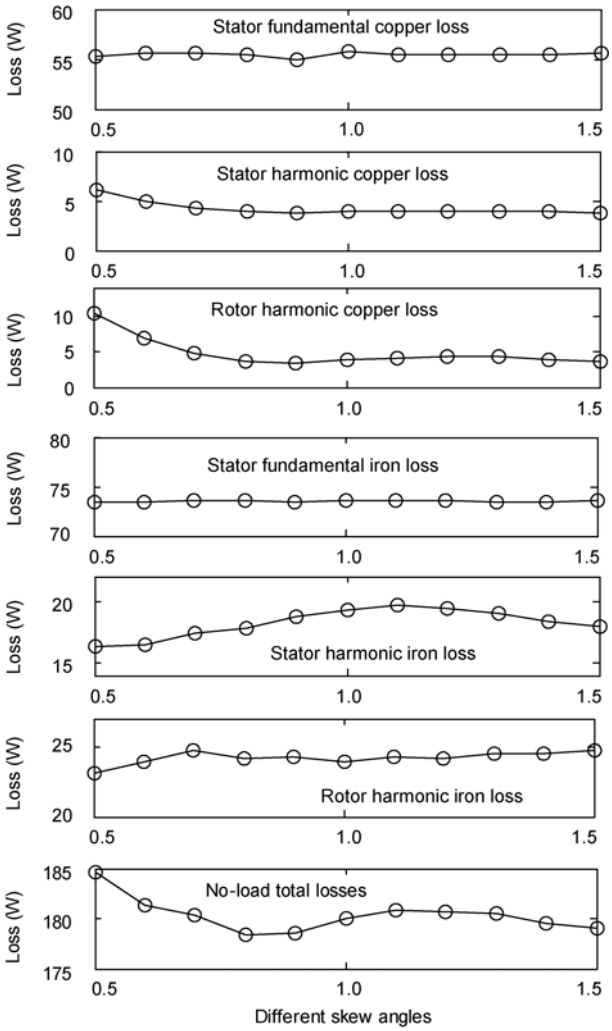

Figure 8 Influence of different skew angles on no-load losses of 5.5 kW motor.

In conclusion, the value of total motor losses under no-load condition is the smallest when rotor skews are over $0.8l_{tp}$.

5.2 Influence of different skew angles on the losses under full-load condition

Figure 9 shows the changing curve of the influence of different skew angles on the motor losses under full-load condition. Similar to the no-load analysis the abscissa stands for different skew angles (γ), γ=$0.5l_{tp}$–$1.5l_{tp}$. The conclusions are as follows:

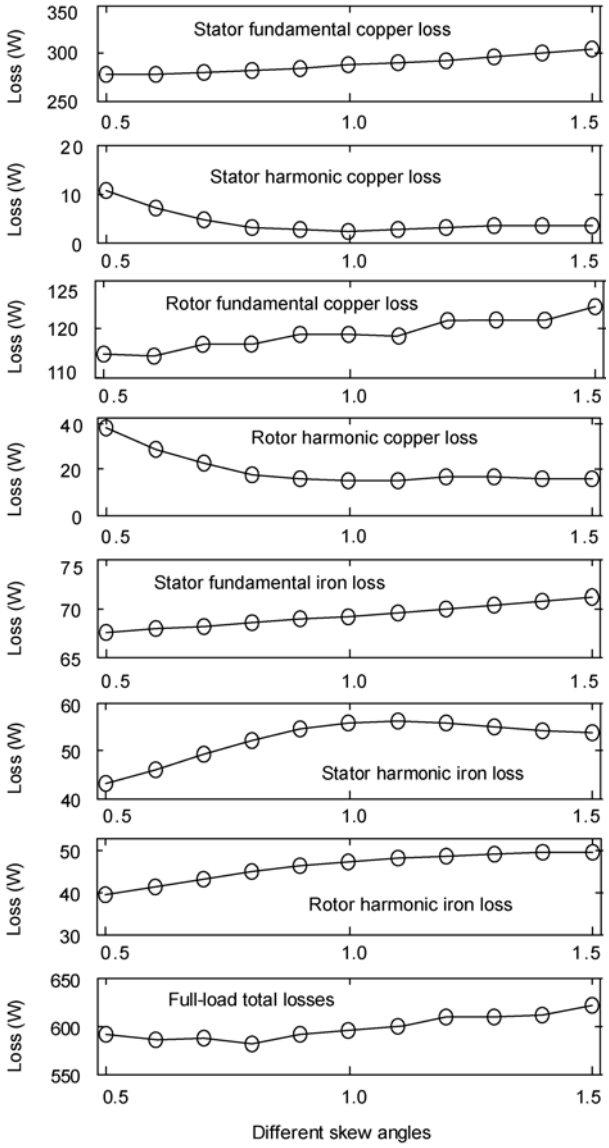

Figure 9 Influence of different skew angles on full-load losses of 5.5 kW motor.

1) Under full-load condition, the fundamental copper loss and iron losses increase as skew angles increase. The main reason is that the core saturation degree along axial direction increases as the demagnetizing effect of the rotor field increases.

2) As in the no-load condition, all of the stator and rotor harmonic copper loss is reduced as the skew angle increases.

3) The variation of stator harmonic iron loss is very similar to that under the no-load condition.

4) The variation of rotor harmonic iron loss is very similar to that under no-load condition, and its increasing trend is more obvious. The main reason for such observed phenomena is that, under full-load condition, the harmonic field caused by the rotor current increasing leads to the increase of rotor harmonic iron loss.

In conclusion, when the rotor skew is $0.8l_{tp}$, the total losses of the motor under full-load condition are the smallest. This corresponds well to the analysis results of the no-load condition.

6 Conclusions

Using a multi-slice field-circuit coupled T-S FEM, the axial field distribution (fundamental & harmonics) in typical locations within stator and rotor cores and its influence on motor losses are systematically studied in this paper. The influence of different skew angles on motor losses is also analyzed. The major conclusions are drawn below.

1) The skewed rotor can reduce harmonic copper loss caused by stator and rotor harmonic currents; however there is also a corresponding increase in the non-uniform field distribution along the axial direction, which leads to greater core saturation and higher iron losses. The influence of skewed rotors on the iron losses depends on load conditions. As the load increases, the degree of core saturation in the sliced motor sections along the axial direction increases and iron losses increase obviously.

2) For the 5.5 kW motor used in this paper, the influence of different skew angles on copper and iron losses is analyzed. The conclusion is that the total motor losses achieve its lowest value when the rotor skew is 0.8 stator tooth pitch, under both no-load and full-load conditions.

The results in this paper can provide useful technical support for proper design of rotor skew for the development of premium motors. The work also lays some theoretical foundation for further research on developing new rotor structures which can reduce the losses and noises caused by slot harmonics.

This work was supported by the National High Technology Research and Development Program of China ("863" Program) (Grant No. 2009AA05Z207).

1 Chen S K. Electrical Machines Design (in Chinese). Beijing: China Machines Press, 2008. 275–277
2 Williamson S, Flack T J, Volschenk A F. Representation of skew in time-stepped two-dimensional finite-element models of electrical machines. IEEE Trans Ind Appl, 1995, 31(5): 1009–1015
3 Jiang J Z, Fu W N. Multi-slice finite element analysis of skewed induction motors (in Chinese). Trans China Electrotech Soc, 1997, 12(5): 11–17
4 Urresty J C, Riba J R, Romeral L, et al. A Simple 2-D finite-element geometry for analyzing surface-mounted synchronous machines with skewed rotor magnets. IEEE Trans Magn, 2010, 46(11): 3948–3954
5 Gyselinck J J C, Vandevelde L, Melkebeek J A A. Multi-slice FE modeling of electrical machines with skewed slots—The skew discretization error. IEEE Trans Magn, 2001, 37(5): 3233–3237
6 Kawase Y, Yamaguchi T, Tu Z P, et al. Effects of skew angle of rotor in squirrel-cage induction motor on torque and loss characteristics. IEEE Trans Magn, 2009, 45(3): 1700–1703
7 McClay C I, Williamson S. The variation of cage motor losses with skew. IEEE Trans Ind Appl, 2000, 36(6): 1563–1570
8 McClay C I, Williamson S. Influence of rotor skew on cage motor

losses. IEE Elect Power Appl, 1998, 145(5): 414–422
9 Kown B I, Kim B T, Jun C S. Analysis of axially non-uniform loss distribution in 3-phase induction motor considering skew effect. IEEE Trans Magn, 1999, 35(3): 1298–1301
10 Kalokiris G D, Kefalas T D, Kladas A G, et al. Special air-gap element for 2-D FEM analysis of electrical Machines accounting for rotor skew. IEEE Trans Magn, 2005, 41(5): 2020–2023
11 Dorrell D G, Holik P J, Rasmussen C B. Analysis and effects of inter-bar current and skew on a long skewed-rotor induction motor for pump applications. IEEE Trans Magn, 2007, 43(6): 2534–2536
12 Dorrell D G, Holik P J, Lombard P, et al. A Multisliced finite-element model for induction machines incorporating interbar current. IEEE Trans Ind Appl, 2009, 45(1): 131–141
13 Zhao H S, Luo Y L, Liu X F, et al. Analysis on no-load iron losses distribution of asynchronous motors with time-stepping finite element method (in Chinese). Proc CSEE, 2010, 30(30): 99–106
14 Zhao H S, Liu X F, Hu J, et al. The influence of wye and delta connection on induction motor losses taking slot opening and skew effect into account. IEEE IEMDC, Miami, USA, 2009. 213–218
15 Zhao H S, Liu X F, Luo Y L, et al. Losses characteristics of cage induction motors under voltage deviation conditions (in Chinese). Electric Mach Contl, 2010, 14(5): 13–19
16 Bertotti G. General properties of power losses in soft ferromagnetic material. IEEE Trans Magn, 1988, 24(1), 621–630
17 Cheng S K, Pei Y L, Zhang P, et al. Fundamental research on the third function of rotating electric machine. Trans China Electrotech Soc, 2007, 22(7): 12–17
18 National Rotational Electrical Machines Standardization Technical Committee. GB/T 1032-2005. Test procedures for three-phase induction motors (in Chinese). Beijing: Standard Press of China, 2005. 6–7
19 Cui X S, Luo Y L, Yang Y L, et al. Energy saving theory and approach for asynchronous motor under the periodically variable running condition (in Chinese). Proc CSEE, 2008, 28(18): 90–97